

The confluence of fractured resonances at points of dynamical, many–body flare

Bitan De,¹ Gabriela Wójtowicz,^{1,2,3} Marek M. Rams,^{1,4,*} Michael Zwolak,^{3,†} and Jakub Zakrzewski^{1,4,‡}

¹*Institute of Theoretical Physics, Jagiellonian University, Łojasiewicza 11, 30-348 Kraków, Poland*

²*Doctoral School of Exact and Natural Sciences, Jagiellonian University, Łojasiewicza 11, 30-348 Kraków, Poland*

³*Biophysical and Biomedical Measurement Group, Microsystems and Nanotechnology Division, Physical Measurement Laboratory, National Institute of Standards and Technology, Gaithersburg, Maryland 20899, USA*

⁴*Mark Kac Center for Complex Systems Research, Jagiellonian University, Łojasiewicza 11, 30-348 Kraków, Poland*

(Dated: August 25, 2023)

Resonant transport occurs when there is a matching of frequencies across some spatial medium, increasing the efficiency of shuttling particles from one reservoir to another. We demonstrate that in a periodically driven, many–body tilted lattice there are sets of spatially fractured resonances. These “emanate” from two essential resonances due to scattering off internal surfaces created when the driving frequency and many–body interaction strength vary, a scattering reminiscent of lens flare. The confluence of these fractured resonances dramatically enhances transport. At one confluence, the interaction strength is finite and the essential resonance arises due to the interplay of interaction with the counter–rotating terms of the periodic drive. The other forms where several paths split by the many–body interaction merge in the non–interacting limit. We discuss the origin and structure of the fractured resonances, as well as the scaling of the conductance on system parameters. These results furnish a new example of the richness of open, driven, many–body systems.

Closed, one–dimensional lattices held at a tilt provide a simple realization of localized dynamics, including for highly excited states, without disorder [1, 2]. An initial framework for understanding such systems links localization to the fragmentation of the Hilbert space and the conservation of a global dipole moment [3, 4]. Theoretical and experimental studies, specifically in the context of cold atoms and trapped atomic ions, have further refined and expanded this initial framework [5–12].

Much less is known for tilted lattices open to an environment, especially in the context of transport where much experimental and theoretical progress has been made in one–, and quasi–one–, dimensional atomic quantum systems [13–29]. For tilted lattices, recent studies have considered time–independent transport in non–interacting [30] and interacting [31] systems, as well as time–dependent transport in non–interacting lattices in contact with structured reservoirs [32]. These works demonstrate interesting phenomena, such as rectification, and highlight challenges in numerical simulation.

In this Letter, we consider transport in periodically driven, interacting tilted lattices, as in Fig. 1. The coupling of these elements—the modulation, the interactions, and the tilt—manifests itself in sets of fractured resonances. These provide transport pathways where resonant regions are spatially separated by barriers resulting from the many–body interaction or mismatch of the driving frequency and tilt. At the confluence of resonances, the conductance markedly increases. We will discuss these pathways, as well as the scaling of the current in different parameter regimes.

The one–dimensional lattice consists of N_S sites where Markovian injection and depletion on the first and last

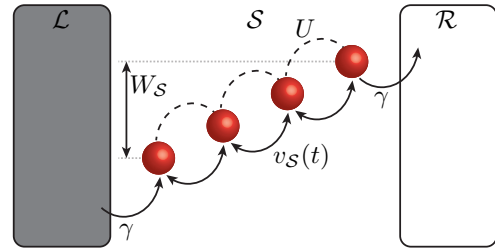


FIG. 1. **Many–body, driven, tilted lattice.** A spinless fermion lattice S of N_S sites is held at a total tilt $W_S = (N_S - 1)\Delta$ and placed between Markovian reservoirs, \mathcal{L} and \mathcal{R} , with injection and depletion, respectively, at rate γ . Fermions interact with a nearest–neighbor, density–density interaction of strength U and tunneling coupling $v_S(t)$ that is periodically driven. The triple—the periodic modulation, the interactions, and the tilt—give rise to the confluence of resonance.

site, respectively, induce transport through the system S . This setup is essentially the large bias limit of the system placed between left (\mathcal{L}) and right (\mathcal{R}) reservoirs, as depicted in Fig. 1. The time evolution of the density matrix, ρ_S , is governed by the equation of motion,

$$\dot{\rho}_S = -i[H_S(t), \rho_S] + \mathcal{D}_S[\rho_S] \equiv \mathcal{L}_S(t)[\rho_S], \quad (1)$$

where $H_S(t)$ is the time–dependent system Hamiltonian and \mathcal{D}_S provides the Markovian injection and depletion on the boundaries. These two contributions combine to give the time–dependent Lindbladian $\mathcal{L}_S(t)$.

In terms of the fermionic creation (annihilation) operators, c_j^\dagger (c_j), on site j , as well as the number operator,

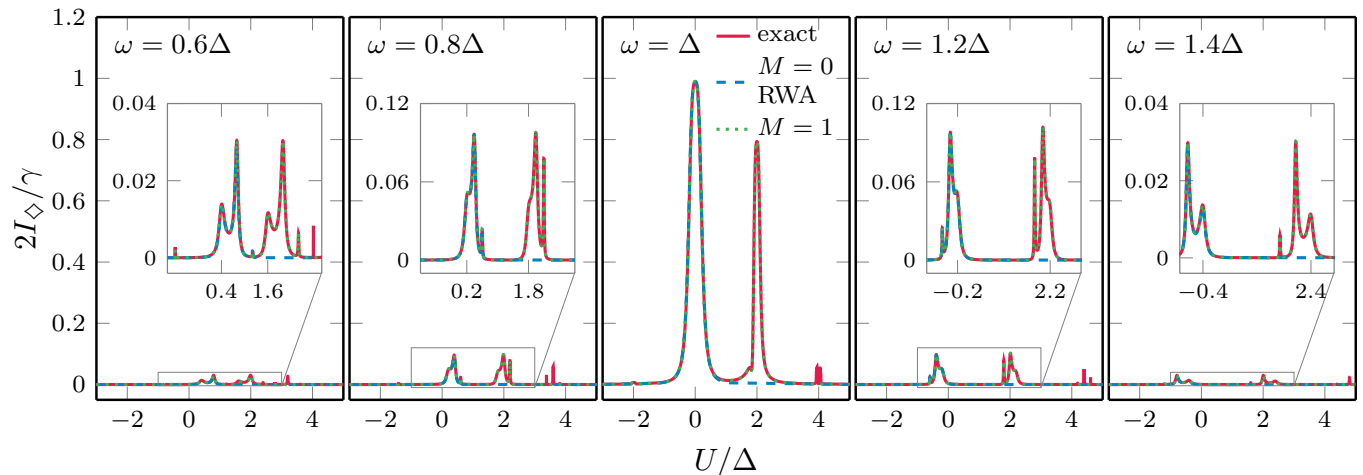


FIG. 2. **Resonance structure.** The mean current as a function of U/Δ for different frequencies ω through a lattice of $N_S = 4$ sites. The red solid lines show the exact mean current, which exhibits a rich resonance structure. At the driving frequency $\omega = \Delta$, the separate resonances merge at $U = 0 \cdot \Delta$ and $U = 2\Delta$. This confluence leads to a large enhancement of the current. The blue dashed lines show the rotating wave approximation (RWA), which accurately captures the small U resonances. The green dotted lines show the approximate result with a single Floquet block, i.e., $M = 1$ in Eq. (9), for the periodic state. The $M = 0$ (equivalent to the RWA) and $M = 1$ results show that the confluence at $U = 2\Delta$ is due to the counter-rotating terms in the Hamiltonian. The other parameters are $\gamma = 0.01\Delta$ and $V_S = 0.1\Delta$.

$n_j = c_j^\dagger c_j$, the system Hamiltonian is

$$H_S(t) = \sum_{j=1}^{N_S} j\Delta n_j + \sum_{j=1}^{N_S-1} U n_j n_{j+1} + v_S(t) \sum_{j=1}^{N_S-1} (c_j^\dagger c_{j+1} + \text{h.c.}), \quad (2)$$

where $v_S(t) = V_S \cos(\omega t)$ and Δ is the site-to-site tilt. The periodically-driven, nearest-neighbor coupling has amplitude V_S and frequency ω , while U is the interaction strength between spinless fermions. The boundary terms are given by the Markovian contribution,

$$\mathcal{D}_S[\rho_S] = \gamma \left(c_1^\dagger \rho_S c_1 - \frac{1}{2} \{c_1^\dagger c_1, \rho_S\} \right) + \gamma \left(c_{N_S} \rho_S c_{N_S}^\dagger - \frac{1}{2} \{c_{N_S}^\dagger c_{N_S}, \rho_S\} \right). \quad (3)$$

There also could be injection and depletion that relax each boundary a fractional occupancy (i.e., between 0 and 1) [29], rather than to either of those limits as in Eq. (3). This does not change the physics in our setup.

We focus on the periodic solutions of the dynamics generated by Eq. (1), i.e., $\rho_S(t+T) = \rho_S(t)$ for sufficiently large time t and period $T = 2\pi/\omega$. This solution comes from the $(1+0i)$ eigenvalue of the Floquet map \mathcal{F}_S ,

$$\mathcal{F}_S = \mathcal{T} e^{\int_0^T \mathcal{L}_S(t) dt}, \quad (4)$$

i.e., the solution $\bar{\rho}_S = \mathcal{F}_S[\bar{\rho}_S]$ is the T -periodic stationary state. Here, \mathcal{T} is the time-ordering operator. Within

this state, we compute the mean current over a cycle,

$$I_\diamond = \frac{1}{T} \int_0^T I_j(t) dt. \quad (5)$$

The current across an interface j , $I_j(t)$, is time- and interface-dependent, but the mean current I_\diamond is independent of j due to particle conservation. The interfacial current is just that flowing from site j to $j+1$ for the one-dimensional lattice,

$$I_j(t) = 2v_S(t) \text{Im} \langle c_j^\dagger c_{j+1} \rangle_t, \quad (6)$$

where $\langle \cdot \rangle_t$ indicates the expectation value of the current at time t within the periodic state $\bar{\rho}_S$.

We concentrate on the resonance structure for a fixed, finite tilt Δ at small V_S and γ , including $V_S/\Delta \ll 1$ to minimally smear bare atomic levels, and scan ω and U . We will consider other regimes, as well as finite bias and fractional occupancy, elsewhere. Figure 2 shows the resonance structure for a four site lattice versus U and for a few values of ω . The rich resonance structure simplifies at $\omega = \Delta$, leading to two large peaks at $U = 0 \cdot \Delta$ and $U = 2\Delta$. These two points—essential resonances or confluence points—form due to the merger of several resonances, as seen in Fig. 3. The magnitude of current suggests a non-additive confluence of the different pathways.

The confluence at $U = 2\Delta$ is surprising, while the confluence at $U = 0 \cdot \Delta$ is in a parameter regime (weak V_S , weak boundary terms, and weak interactions) that should—and is, as we will see—be well described by the rotating wave approximation (RWA). This approximation works well for the fully non-interacting ($U = 0 \cdot \Delta$)

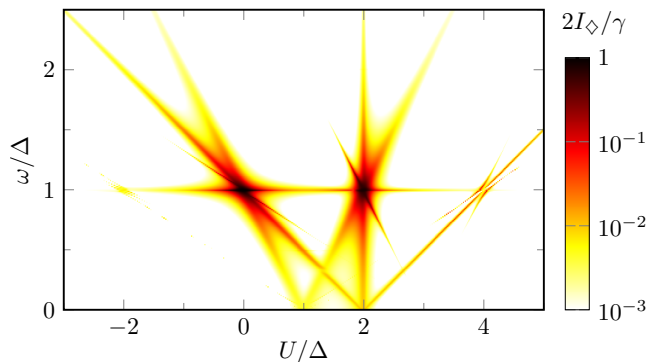


FIG. 3. **Confluence of resonance.** The resonance locations, depicted via the color scale on the right, versus the driving frequency ω and many-body interaction strength U . Several resonances trace paths that relate ω and U . These resonances come together at two confluence points ($U = 0 \cdot \Delta$ and $U = 2\Delta$). At $U = 2\Delta$, the resonances at $\omega = U - \Delta$ and $\omega = 3\Delta - U$ merge with the (driving-independent) $U = 2\Delta$ resonance and the (many-body-independent) $\omega = \Delta$ resonance. At $U = 0 \cdot \Delta$, the resonances at $\Delta - U$ and $\Delta - U/2$, and a very fine resonance at $\Delta - U/3$, merge with the $\omega = \Delta$ resonance. As in Fig. 2, we use $\gamma = 0.01\Delta$ and $V_S = 0.1\Delta$.

lattice [32]. We will extend it to non-zero U in the neighborhood of the non-interacting confluence. The merger occurs at the single-photon resonance, $\omega = \Delta$, i.e., when the driving frequency is equal to the site-to-site step. In the rotating frame ($a_j \equiv e^{i\omega t} c_j$), the Hamiltonian is

$$\begin{aligned} \check{H}_S(t) &= \sum_{j=1}^{N_S} j(\Delta - \omega) n_j + \sum_{j=1}^{N_S-1} U n_j n_{j+1} \\ &+ \frac{V_S}{2} \sum_{j=1}^{N_S-1} \left[a_j^\dagger a_{j+1} (1 + e^{-2i\omega t}) + \text{h.c.} \right] \quad (7) \\ &\equiv H_0 + H_1 e^{-2i\omega t} + H_1^\dagger e^{2i\omega t}, \end{aligned}$$

with $H_1 = \sum_j (V_S/2) a_j^\dagger a_{j+1}$. The RWA drops the rapidly rotating terms, $e^{\pm 2i\omega t}$, making the problem time independent. More generally, the Floquet approach provides an elegant method of treating the periodic drive [33] by looking for a NESS that is a Fourier series

$$\bar{\rho}_S = \sum_{m=-M}^M \rho_m e^{2im\omega t}. \quad (8)$$

The parameter M is a control where the RWA corresponds to $M = 0$ and the exact solution to $M \rightarrow \infty$. In the rotated frame, the NESS (more precisely, the approximation of a true NESS using finite M) satisfies

$$[H_0, \rho_m] + [H_1, \rho_{m+1}] + [H_1^\dagger, \rho_{m-1}] + 2m\omega \rho_m + i\mathcal{D}_S[\rho_m] = 0, \quad (9)$$

with $m \in [-M, M]$, which amounts to finding $(0 + 0i)$ eigenvector of a $(2M+1)4^{N_S}$ dimensional square matrix.

Figure 2 shows the current within the RWA as blue dashed lines. The small U/Δ peaks (those belonging to the $U = 0 \cdot \Delta$ confluence point) are captured with the RWA. This is contrary to the peaks contributing to the $U = 2\Delta$ confluence, indicating that they require the “counter-rotating” terms in \check{H}_S , i.e., its understanding requires the full time dependence of Eq. (7).

Confluence of resonances at $U = 0 \cdot \Delta$. Since the RWA captures this confluence, we can safely drop the counter-rotating terms, making the lattice a uniform, non-interacting lattice between two Markovian reservoirs when $\omega = \Delta$. The current is thus [23, 34]

$$I_\diamond = \frac{\gamma}{2} \frac{V_S^2}{V_S^2 + \gamma^2}, \quad (10)$$

which uses that the RWA hopping is $V_S/2$. When $\gamma \ll V_S$, the current will approach a maximal possible value of $\gamma/2$. This occurs because the setup is well described by two resistors, one with resistance $1/\gamma$ at the left boundary and one with $1/\gamma$ at the right boundary. The lattice itself has effectively zero resistance in this limit, as the uniform, non-interacting lattice forms a fully transmissive ballistic channel. Thus, the whole setup is essentially two resistors in series adding up to a total resistance of $2/\gamma$ [35].

When $V_S \ll \gamma$, the current is $V_S^2/2\gamma$. This dependence occurs due to the overdamping of the first and last sites in direct analogy to Kramers’ turnover within extended reservoir approaches for quantum [36–43] and classical [44–47]. In that context, it has been proven that the current decays as $1/\gamma$ for (time-independent) non-interacting or many-body quantum transport [36, 39]. The Markovian injection and depletion is so strong that particles can not move away from or toward the relaxed modes (here, the boundary sites) fast enough. In other words, the coherence is damped, suppressing the current. This scenario can also be considered as two resistors but now between the two boundary sites and the “bulk.”

In the neighborhood of the confluence, the resonances for small U are also well-reproduced by the RWA, see Fig. 2, including for ω away from Δ . Thus, to understand the fracturing, we can analyze the state structure of the time-independent RWA Hamiltonian. We focus on $N_S = 4$, as this is the smallest N_S that has the general features of fracturing ($N_S = 3$ has a quasi-confluence but does not have the general features of larger N_S). One of the fractured resonances, at $\omega = \Delta$, is independent of the many-body interaction. It has a homogeneous, single-particle channel, similar to $U = 0 \cdot \Delta$ (a closely related model—XXZ—remains ballistic for $|U| < V_S$ [24]). The other channels, though, occur at $\omega = \Delta - U$ and $\omega = \Delta - U/2$, and a very fine resonance at $\omega = \Delta - U/3$.

Considering $\omega = \Delta - U$, there are single photon transitions between Fock states $\bullet\bullet\circ\circ$ and $\bullet\circ\bullet\circ$ (using \bullet for occupied and \circ for unoccupied sites). These states have atomic frequencies $3(\Delta - \omega) + U$ and $4(\Delta - \omega) + U$

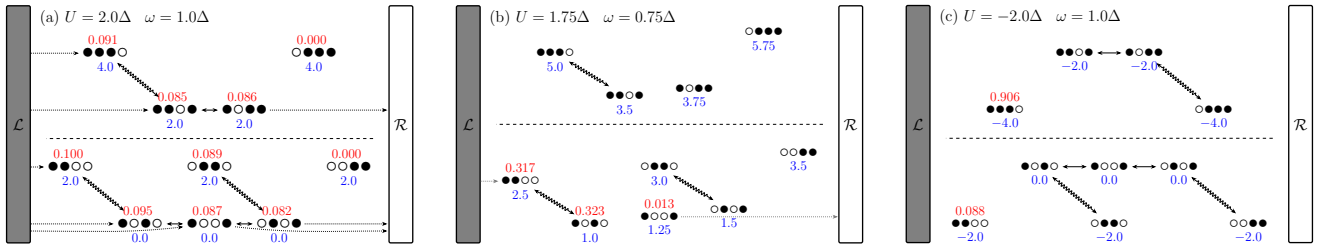


FIG. 4. **State structure of two- and three-particle sectors in the rotated frame, Eq. (7).** Bare frequencies without hopping are given in blue. State occupations are in red (for $V_S = 0.1\Delta$ and $\gamma = 0.01\Delta$). (a) At confluence ($\omega = \Delta$ and $U = 2\Delta$), a resonant path is formed by a combination of one-photon (horizontal arrows) and counter-rotation driven (wavy arrows) resonances. (b) Away from confluence, some resonant transitions remain but they are spatially fractured. Transport requires flow through intermediate, non-resonant states. (c) At $U = -2\Delta$, the state structure exactly maps to $U = +2\Delta$ but with injection and depletion swapped in Eq. (3). The directional character of three-photon processes brakes the spatial symmetry, leading to a NESS where the state $\bullet\bullet\bullet\circ$ is the dominant component, blocking transport across the lattice.

the rotating frame, respectively, which become resonant when $\omega = \Delta - U$. However, *this is a fractured resonance*, as the lattice no longer has a uniform onsite frequency. For transport to occur across the whole system, fermions must overcome a barrier after, e.g., the resonance from $\bullet\bullet\bullet\circ$ to $\bullet\circ\bullet\circ$. That is, there is a barrier—and dependence on V_S —to go into $\bullet\circ\bullet\circ$, which then allows the particle into the right reservoir and contribute to the NESS current. The three particle sector, via the states $\bullet\bullet\bullet\circ$ and $\bullet\circ\bullet\circ$, also contributes to the fractured resonance via a single-photon process.

The other two fractured resonances require two- and three-photon processes, respectively. For $\omega = \Delta - U/2$, the transition is between $\bullet\bullet\bullet\circ$ and $\bullet\circ\bullet\circ$, and has a magnitude proportional to V_S^2 , which is suppressed compared to the first order resonant coupling. For $\omega = \Delta - U/3$, the transition is between $\bullet\bullet\bullet\circ$ and $\circ\bullet\bullet\circ$, which is further suppressed with a higher power of V_S .

Confluence of resonances at $U = 2\Delta$. The resonances that meet at $U = 2\Delta$ have a different character. They are not present within the RWA, even when V_S/Δ is small, as their existence is related to counter-rotating terms in \check{H}_S (for a review of other cases where the RWA breaks down, see Ref. [48]). However, similar to the $U = 0 \cdot \Delta$ confluence, there are several fractured resonances. Figure 4a shows the state structure at confluence. An extensive channel—one that spans the whole lattice—opens up in both the two- and three-particle sectors. The counter-rotating terms, as shown by wavy arrows in the figure, connect the states with neighboring particles to transporting states. For instance, the counter-rotation connects $\bullet\bullet\bullet\circ$ and $\bullet\circ\bullet\circ$, where the latter can then resonantly shuttle one particle to the right boundary, creating a full path through the lattice. The connectivity, where neighboring particles with a many-body interaction can separate, allows the lattice to stay open and efficiently transport particles across the system.

In the neighborhood of confluence, specifically along the $\omega = U - \Delta$ fractured resonance, Fig. 4b shows how

the counter-rotating terms create local resonances—ones that are spatially disconnected—within the two-particle sector. Transport across the whole lattice has to flow through intermediate states with some barrier. Current still flows at finite N_S but drops rapidly as V_S decreases and N_S increases, see the Fig. 5 inset. At one of the other fractured resonances, $U = 2\Delta$, a two-photon resonance between $\bullet\bullet\bullet\circ$ and $\bullet\circ\bullet\circ$ facilitates transfer across the lattice for arbitrary ω . The linking of all the resonances— $\omega = U - \Delta$, $\omega = 3\Delta - U$, $U = 2\Delta$, and $\omega = \Delta$ —at confluence leads to a giant increase of the current.

Rectification. While we observe a confluence at $U = 2\Delta$, no such effect occurs for $U = -2\Delta$, although the state structure seems similar, see Fig. 4c. This is due to the fact that H_1 in Eq. (7) facilitates transport to higher frequency states to the left, while H_1^\dagger facilitates transport to lower frequency states to the right. This breaks the spatial symmetry of the lattice, where counter-rotation permits $U = +2\Delta$ to carry a current from left to right, matching the Markovian injection and depletion in Eq. (1). For $U = -2\Delta$, counter-rotation permits a current from right to left but this is opposite to the induced current in Eq. (1) and the system gets filled into a blocked state $\bullet\bullet\bullet\circ$. Swapping the Markovian injection and depletion (but holding the tilt in the positive direction) would result in the confluence being at $U = -2\Delta$ and, then, $U = 2\Delta$ would fill to a blocked state $\circ\bullet\bullet\circ$. The system thus displays strong rectification, although its origin is different from the rectification in *time-independent* lattices [31, 49, 50].

Increasing N_S . In Fig. 5, we show how the current depends on V_S/γ for several N_S and γ for the many-body confluence point. There is a scaling regime where

$$I_\diamond \sim \frac{V_S^2}{\gamma} \quad (11)$$

for all N_S reachable with exact diagonalization. This parallels the $U = 0 \cdot \Delta$ confluence, suggesting, at minimum, an extensive transport pathway that spans the

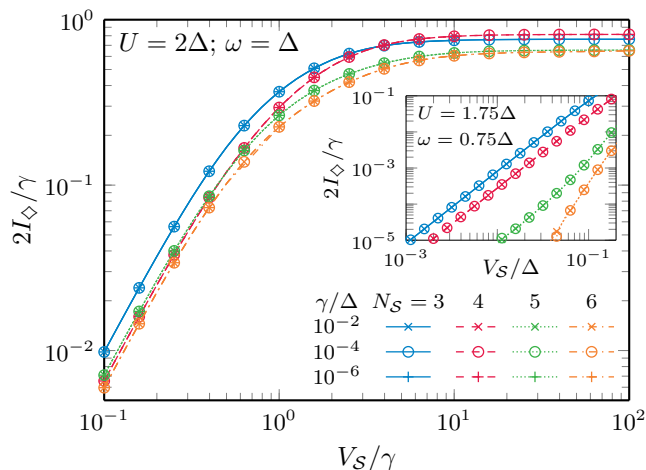


FIG. 5. **Current at the many-body confluence.** The current versus V_S/γ demonstrates that there is scaling limit where the current is proportional to V_S^2/γ . This parallels the behavior at non-interacting confluence ($U = 0 \cdot \Delta$ and $\omega = \Delta$) where the current is given by Eq. (10) and takes on the scaling V_S^2/γ for small V_S . For large V_S/γ , the current comes close to its maximal value and with a weak dependence on N_S . The inset shows qualitatively different behavior away from the confluence point, where the current vanishes with a higher power of V_S and has a strong dependence on N_S .

whole lattice. The overdamped boundary sites then dominate the behavior rather than the system itself, regardless of length. For larger V_S/γ , the current approaches the maximal value of $\gamma/2$. However, there is some weak dependence on N_S , unlike the confluence at $U = 0 \cdot \Delta$ where the current is independent of N_S since there is a purely ballistic channel. The scaling, nevertheless, needs to be determined for even larger N_S , as there may be a transition to different behavior (e.g., to a constant or to a power law) as the lattice length increases. Away from confluence, the spatial fracturing grows with N_S , as expected and will be described elsewhere. We note, though, that the current drops even more dramatically than for $N_S = 4$, as the spatially fracturing brings in multiple interfaces that interrupt current flow. In other words, the “flare” contracts inward towards the confluence point.

Conclusions. We have analyzed fermionic transport through a tilted lattice with harmonically driven couplings. For weak interactions, there are several fractured resonances. These merge at the non-interacting confluence where the driving frequency matches the lattice tilt. Quite unexpectedly, a second confluence occurs for strong interactions, one that is not captured by the rotating wave approximation. This confluence occurs because the counter-rotating terms allow extensive transport channels to open. The effect is robust for the regimes studied and may dominate transport for longer systems.

We gratefully acknowledge Polish high-performance computing infrastructure PLGrid (HPC Centers: ACK

Cyfronet AGH) for providing computer facilities and support within computational grant no. PLG/2023/016370. This research has been supported by the National Science Centre (Poland) under project 2019/35/B/ST2/00034 (B.D.), 2020/38/E/ST3/00150 (G.W. and M.M.R.) and under the OPUS call within the WEAVE program 2021/43/I/ST3/01142 (J.Z.). G.W. acknowledges the Fulbright Program. The research has been supported by a grant from the Priority Research Area (DigiWorld) under the Strategic Programme Excellence Initiative at Jagiellonian University (J.Z., M.M.R.). No part of this work was written by artificial intelligence.

* marek.rams@uj.edu.pl

† mpz@nist.gov

‡ jakub.zakrzewski@uj.edu.pl

- [1] E. van Nieuwenburg, Y. Baum, and G. Refael, From Bloch oscillations to many-body localization in clean interacting systems, *Proc. Natl. Acad. Sci. U.S.A.* **116**, 9269 (2019).
- [2] M. Schulz, C. Hooley, R. Moessner, and F. Pollmann, Stark Many-Body localization, *Phys. Rev. Lett.* **122**, 040606 (2019).
- [3] V. Khemani, M. Hermele, and R. Nandkishore, Localization from Hilbert space shattering: From theory to physical realizations, *Phys. Rev. B* **101**, 174204 (2020).
- [4] P. Sala, T. Rakovszky, R. Verresen, M. Knap, and F. Pollmann, Ergodicity breaking arising from Hilbert space fragmentation in dipole-conserving Hamiltonians, *Phys. Rev. X* **10**, 011047 (2020).
- [5] S. R. Taylor, M. Schulz, F. Pollmann, and R. Moessner, Experimental probes of Stark many-body localization, *Phys. Rev. B* **102**, 054206 (2020).
- [6] T. Chanda, R. Yao, and J. Zakrzewski, Coexistence of localized and extended phases: Many-body localization in a harmonic trap, *Phys. Rev. Research* **2**, 032039 (2020).
- [7] R. Yao, T. Chanda, and J. Zakrzewski, Many-body localization in tilted and harmonic potentials, *Phys. Rev. B* **104**, 014201 (2021).
- [8] R. Yao, T. Chanda, and J. Zakrzewski, Nonergodic dynamics in disorder-free potentials, *Ann. Phys. (N. Y.)* **435**, 168540 (2021).
- [9] E. V. H. Doggen, I. V. Gornyi, and D. G. Polyakov, Stark many-body localization: Evidence for Hilbert-space shattering, *Phys. Rev. B* **103**, L100202 (2021).
- [10] W. Morong, F. Liu, P. Becker, K. S. Collins, L. Feng, A. Kyprianidis, G. Pagano, T. You, A. V. Gorshkov, and C. Monroe, Observation of Stark many-body localization without disorder, *Nature* **599**, 393 (2021).
- [11] S. Scherg, T. Kohlert, P. Sala, F. Pollmann, B. Hebbe Madhusudhana, I. Bloch, and M. Aidelsburger, Observing non-ergodicity due to kinetic constraints in tilted Fermi-Hubbard chains, *Nat. Commun.* **12**, 4490 (2021).
- [12] T. Kohlert, S. Scherg, P. Sala, F. Pollmann, B. Hebbe Madhusudhana, I. Bloch, and M. Aidelsburger, Exploring the regime of fragmentation in strongly tilted Fermi-Hubbard chains, *Phys. Rev. Lett.* **130**, 010201 (2023).

- [13] J.-P. Brantut, J. Meineke, D. Stadler, S. Krinner, and T. Esslinger, Conduction of ultracold fermions through a mesoscopic channel, *Science* **337**, 1069 (2012).
- [14] C.-C. Chien, M. Zwolak, and M. Di Ventra, Bosonic and fermionic transport phenomena of ultracold atoms in one-dimensional optical lattices, *Phys. Rev. A* **85**, 041601 (2012).
- [15] J.-P. Brantut, C. Grenier, J. Meineke, D. Stadler, S. Krinner, C. Kollath, T. Esslinger, and A. Georges, A thermoelectric heat engine with ultracold atoms, *Science* **342**, 713 (2013).
- [16] C.-C. Chien, D. Gruss, M. D. Ventra, and M. Zwolak, Interaction-induced conducting–non-conducting transition of ultra-cold atoms in one-dimensional optical lattices, *New J. Phys.* **15**, 063026 (2013).
- [17] S. Kohler, J. Lehmann, and P. Hänggi, Driven quantum transport on the nanoscale, *Phys. Rep.* **406**, 379 (2005).
- [18] S. Krinner, D. Stadler, D. Husmann, J.-P. Brantut, and T. Esslinger, Observation of quantized conductance in neutral matter, *Nature* **517**, 64 (2015).
- [19] S. Krinner, M. Lebrat, D. Husmann, C. Grenier, J.-P. Brantut, and T. Esslinger, Mapping out spin and particle conductances in a quantum point contact, *Proc. Natl. Acad. Sci. U.S.A.* **113**, 8144 (2016).
- [20] S. Krinner, T. Esslinger, and J.-P. Brantut, Two-terminal transport measurements with cold atoms, *J. Phys.: Condens. Matter* **29**, 343003 (2017).
- [21] S. Häusler, S. Nakajima, M. Lebrat, D. Husmann, S. Krinner, T. Esslinger, and J.-P. Brantut, Scanning gate microscope for cold atomic gases, *Phys. Rev. Lett.* **119**, 030403 (2017).
- [22] D. Gruss, C.-C. Chien, J. T. Barreiro, M. D. Ventra, and M. Zwolak, An energy-resolved atomic scanning probe, *New J. Phys.* **20**, 115005 (2018).
- [23] D. Karevski and T. Platini, Quantum Nonequilibrium Steady States Induced by Repeated Interactions, *Phys. Rev. Lett.* **102**, 207207 (2009).
- [24] T. Prosen, Exact nonequilibrium steady state of a strongly driven open XXZ chain, *Phys. Rev. Lett.* **107**, 137201 (2011).
- [25] T. Prosen, Open XXZ spin chain: Nonequilibrium steady state and a strict bound on ballistic transport, *Phys. Rev. Lett.* **106**, 217206 (2011).
- [26] M. Žnidarič, Spin transport in a one-dimensional anisotropic Heisenberg model, *Phys. Rev. Lett.* **106**, 220601 (2011).
- [27] D. Karevski, V. Popkov, and G. M. Schütz, Exact matrix product solution for the boundary-driven Lindblad XXZ chain, *Phys. Rev. Lett.* **110**, 047201 (2013).
- [28] B. Bertini, F. Heidrich-Meisner, C. Karrasch, T. Prosen, R. Steinigeweg, and M. Žnidarič, Finite-temperature transport in one-dimensional quantum lattice models, *Rev. Mod. Phys.* **93**, 025003 (2021).
- [29] G. T. Landi, D. Poletti, and G. Schaller, Nonequilibrium boundary-driven quantum systems: Models, methods, and properties, *Rev. Mod. Phys.* **94**, 045006 (2022).
- [30] J. M. A. Pinho, J. P. S. Pires, S. M. João, B. Amorim, and J. M. V. P. Lopes, From Bloch oscillations to a steady-state current in strongly biased mesoscopic devices, *Phys. Rev. B* **108**, 075402 (2023).
- [31] J. J. Mendoza-Arenas and S. R. Clark, Giant rectification in strongly-interacting boundary-driven tilted systems, *arXiv:2209.11718* (2022).
- [32] B. De, G. Wójtowicz, J. Zakrzewski, M. Zwolak, and M. M. Rams, Transport in a periodically driven tilted lattice via the extended reservoir approach: Stability criterion for recovering the continuum limit, *Phys. Rev. B* **107**, 235148 (2023).
- [33] J. H. Shirley, Solution of the Schrödinger equation with a Hamiltonian periodic in time, *Phys. Rev.* **138**, B979 (1965).
- [34] M. Žnidarič, A matrix product solution for a nonequilibrium steady state of an XX chain, *J. Phys. A: Math. Theor.* **43**, 415004 (2010).
- [35] We are operating at infinite bias and thus there is no notion of current being proportional to voltage. Moreover, a four probe setup is not sufficient due to the lack of resistance in the system. Nevertheless, the boundary driving terms add like resistors in series [36].
- [36] D. Gruss, K. A. Velizhanin, and M. Zwolak, Landauer’s formula with finite-time relaxation: Kramers’ crossover in electronic transport, *Sci. Rep.* **6**, 24514 (2016).
- [37] J. E. Elenewski, D. Gruss, and M. Zwolak, Communication: Master equations for electron transport: The limits of the Markovian limit, *J. Chem. Phys.* **147**, 151101 (2017).
- [38] D. Gruss, A. Smolyanitsky, and M. Zwolak, Communication: Relaxation-limited electronic currents in extended reservoir simulations, *J. Chem. Phys.* **147**, 141102 (2017).
- [39] M. Zwolak, Analytic expressions for the steady-state current with finite extended reservoirs, *J. Chem. Phys.* **153**, 224107 (2020).
- [40] M. Zwolak, Comment on ”Quantum transport with electronic relaxation in electrodes: Landauer-type formulas derived from the driven Liouville-von Neumann approach” [The Journal of Chemical Physics 153, 044103 (2020)], *arXiv:2009.04466* (2020).
- [41] G. Wójtowicz, J. E. Elenewski, M. M. Rams, and M. Zwolak, Dual current anomalies and quantum transport within extended reservoir simulations, *Phys. Rev. B* **104**, 165131 (2021).
- [42] J. E. Elenewski, G. Wójtowicz, M. M. Rams, and M. Zwolak, Performance of reservoir discretizations in quantum transport simulations, *J. Chem. Phys.* **155**, 124117 (2021).
- [43] G. Wójtowicz, A. Purkayastha, M. Zwolak, and M. M. Rams, Accumulative reservoir construction: Bridging continuously relaxed and periodically refreshed extended reservoirs, *Phys. Rev. B* **107**, 035150 (2023).
- [44] K. A. Velizhanin, C.-C. Chien, Y. Dubi, and M. Zwolak, Driving denaturation: Nanoscale thermal transport as a probe of DNA melting, *Phys. Rev. E* **83**, 050906 (2011).
- [45] C.-C. Chien, K. A. Velizhanin, Y. Dubi, and M. Zwolak, Tunable thermal switching via DNA-based nano-devices, *Nanotechnology* **24**, 095704 (2013).
- [46] C.-C. Chien, S. Kouachi, K. A. Velizhanin, Y. Dubi, and M. Zwolak, Thermal transport in dimerized harmonic lattices: Exact solution, crossover behavior, and extended reservoirs, *Phys. Rev. E* **95**, 012137 (2017).
- [47] C.-C. Chien, K. A. Velizhanin, Y. Dubi, B. R. Ilic, and M. Zwolak, Topological quantization of energy transport in micromechanical and nanomechanical lattices, *Phys. Rev. B* **97**, 125425 (2018).
- [48] A. Frisk Kockum, A. Miranowicz, S. De Liberato, S. Savasta, and F. Nori, Ultrastrong coupling between light and matter, *Nat. Rev. Phys.* **1**, 19 (2019).

- [49] G. T. Landi, E. Novais, M. J. De Oliveira, and D. Karevski, Flux rectification in the quantum X X Z chain, *Phys. Rev. E* **90**, 042142 (2014).
- [50] V. Balachandran, G. Benenti, E. Pereira, G. Casati, and D. Poletti, Perfect Diode in Quantum Spin Chains, *Phys. Rev. Lett.* **120**, 200603 (2018).